



Modulating optical and electrochemical properties of perylene dyes by twisting aromatic π -system structures

Ying Wang, Qi Zhang, Junbo Gong^{**}, Xin Zhang^{*}

School of Chemical Engineering and Technology, Collaborative Innovation Center of Chemistry Science and Engineering, Tianjin University, Tianjin, 300072, China

ARTICLE INFO

Keywords:

Fluorescence
Dyes
Perylene bisimides
Fluorescence quantum yields
Fluorescence probes
Polarization

ABSTRACT

Three highly fluorescent perylene bisimide dyes were synthesized, where aromatic π -system structures are twisted to different degree by steric hindrance of two or four substitution groups at bay position. Light-emitting colours of these dye solutions can be modulated from green, yellow to red, and their fluorescence quantum yields increase up to approximate 100% with increasing the π -system twisting, which can be considered for new class of wavelength-tunable dye lasers. π -Twisted dyes are more sensitive to microenvironment changes. Thus, they are better fluorescence probe and sensory materials than planar dyes. Electrochemical cyclic voltammetry measurements revealed that these dyes are suitable for n-type optoelectrical devices and materials. These dye solids display near infra-red emission at 600–850 nm. Owing to strong π - π stacking interaction, planar dye solid loses its outstanding optical properties compared to its solution. In contrast, π -twisted dye solids retain their excellent optical properties including narrow emission bands and relatively high fluorescence quantum yields due to the suppression of π - π stacking interaction. Exceptional fluorescence polarization phenomena were observed for these π -twisted dye solids. These optical results revealed that π -twisted perylene bisimide dyes are more excellent optical materials than planar dyes.

1. Introduction

The information determining optical and optoelectronic properties of functional dye materials is generally encoded in chemical structures, molecular shapes and arrangements [1–6]. Therefore, a deep understanding of the structure-property relationship is significant to rational design of π -system molecules to achieve high performance optical and optoelectronic devices and materials [7–10]. Optical materials based on π -system dyes recently have attracted much interest for their diverse applications such as bio-labeling [11,12], dye lasers [13], light-emitting diodes [14], photovoltaic cells [15–21], organic field-effect transistors [22,23], sensors [24–29]. Perylene bisimide dyes are polycyclic, aromatic, extended π -conjugated molecules consisting of five fused benzene rings, which contains the smallest π -system graphene fragment [30,31]. The strong tendency toward π - π stacking of aromatic π -system dyes leads to their low solubility and dramatically optical quenching in the solid state, which severely limits their practical applications. Thus, a chemical modification method was recently developed to obtain excellent optical properties of solid states by preventing π - π stacking interaction, that is,

incorporation of large bulky substituent groups at imide or bay-position of perylene dyes [32–34]. Although the syntheses of π -twisted perylene dyes have been frequently reported from organic and supramolecular chemists [35], the purpose of most of these syntheses is to improve the solubility of perylene dyes. The systematic studies on the effect of aromatic π -system twisting on optical behaviors are scarce.

Generally, the twisting of aromatic π -systems is challenging, and a large degree of twisting may even destroy conjugated π -system structure [36]. In our earlier work, we investigated the relationship between aggregation morphologies and molecular structures, and reported the precision morphology control of supramolecular polymers by twisting conjugated π -system plane. Planar π -system dyes self-assembled into light-emitting rigid rod-like supramolecular polymers by strong π - π stacking [37], and twisted π -system dyes self-assembled into flexible worm-like supramolecular polymers [38]. We further developed their functionalization and reported white-light emitting vesicles [25] and superhelix [39]. These exceptional optical and optoelectronic properties motivated us to explore the property-structure relationship. In this work, we designed and synthesized three perylene dyes with different twist

* Corresponding author.

** Corresponding author.

E-mail addresses: junbo_gong@tju.edu.cn (J. Gong), xzhangchem@tju.edu.cn (X. Zhang).

<https://doi.org/10.1016/j.dyepig.2021.109261>

Received 21 December 2020; Received in revised form 2 February 2021; Accepted 14 February 2021

Available online 23 February 2021

0143-7208/© 2021 Elsevier Ltd. All rights reserved.

angles between two naphthalene units, and investigated their optical and electrochemical properties of solution and solid states. In particular, we demonstrate the optical property modulation of functional dye materials from π -twisting viewpoint.

2. Experimental section

2.1. Synthesis

N,N'-di(1,3-bis(2-(2-(2-methoxyethoxy)ethoxy)ethoxy)prop-2-yl)perylene-3,4:9,10-tetra carboxylic bisimide (**1**): 2,5,8,11,15,18,21,24-Octaoxa-13-pentacosane-amine (1.055 g, 2.75 mmol), perylene-3,4:9,10-tetracarboxylic acid bisanhydride (400 mg, 1.02 mmol) and zinc acetate (0.06 g) were mixed with imidazole (5 g). The reaction mixture was stirred at 150 °C for 6 h under argon. After cooling to room temperature, 2 N HCl (30 mL) was added to the above mixture. The solution was extracted with 50 mL chloroform for three times. The combined chloroform solution was dried with anhydrous MgSO₄ and then the solvent was evaporated. The crude product was further purified by silica gel column chromatography with dichloromethane/methanol ((96/4) → (93/7)) as eluent to give final product (178 mg). Yield: 16%. ¹H NMR (400 MHz, CDCl₃, ppm, Fig. S2): δ = 8.48 (dd, 8H, ArH), 5.75–5.64 (m, 2H, 2-CH(CH₂)₂), 4.20, 3.97 (dd, 8H, 2-CH(CH₂)₂), 3.75–3.45 (m, 48H, 2-OCH₂), 3.31 (s, 12H, 4-OCH₃). ¹³C NMR (CDCl₃, ppm, Fig. S3): δ = 163.81, 134.42, 131.40, 129.46, 126.25, 123.46, 123.02, 71.94, 70.51, 69.40, 58.98, 52.29. MS (MALDI-TOF, Fig. S4) calculated for C₅₈H₇₈N₂O₂₀, 1122.51; found: 1145.63 [M + Na⁺]. IR: $\tilde{\nu}$ (cm⁻¹) = 2916.3, 2867.4, 1693.8, 1653.1, 1593.1, 1574.8, 1435.8, 1403.5, 1343.1, 1249.9, 1100.1, 857.7. UV-vis absorption (dichloromethane): λ_{ab} (ϵ , M⁻¹cm⁻¹) = 525 nm (8.43 × 10⁴), 489 nm (5.13 × 10⁴), 458 nm (1.92 × 10⁴), [**1**] = 2 × 10⁻⁶ M. Fluorescence (dichloromethane, λ_{ex} = 450 nm): λ_{em} = 534 nm, [**1**] = 2 × 10⁻⁶ M.

N,N'-dicyclohexyl-1,7-di(3-methoxyphenoxy)perylene-3,4:9,10-tetracarboxylic acid bisimide (**2**): *N,N'*-dicyclohexyl-1,7-dibromoperylene-3,4:9,10-tetracarboxylic dianhydride (1 g, 1.4 mmol), K₂CO₃ (606 mg, 4.39 mmol) and 3-methoxyphenol (1.51 g, 12.2 mmol) were added into *N*-methyl pyrrolidone (NMP, 60 mL). The reaction mixture was stirred at 120 °C for 1 h, then was cooled to room temperature. HCl aqueous (100 mL, 8 vol-%) was slowly added dropwise to the reaction solution with stirring, and the crude product precipitated out and was washed with water then dried under vacuum. The crude product was purified by silica gel column chromatography with dichloromethane/n-hexane (2/1) as eluent to give red solid (0.73 g). Yield: 65%. ¹H NMR (400 MHz, CDCl₃, ppm, Fig. S6): δ = 9.50 (d, 2H, ArH), 8.58 (d, 2H, ArH), 8.26 (d, 2H, ArH), 7.37–7.28 (m, 2H, ArH), 6.84–6.75 (m, 2H, ArH), 6.71 (dd, 4H, ArH), 5.08–4.88 (m, 2H, 2-CH(CH₂)₂), 3.83 (s, 6H, 2-CH₃), 2.61–2.39 (m, 4H, -CH(CH₂)₂), 1.88 (d, 4H, -CH(CH₂)₂), 1.78–1.21 (m, 12H, 6-CH₂). ¹³C NMR (CDCl₃, ppm, Fig. S7): δ = 163.80, 163.36, 161.61, 156.32, 155.02, 133.25, 131.02, 130.29, 129.22, 128.81, 125.35, 124.52, 124.40, 123.95, 122.88, 111.54, 110.52, 105.94, 55.60, 54.13, 29.18, 26.58, 25.50. HRMS (ESI, Fig. S8): calculated for C₅₀H₄₂N₂O₈: 798.2941; found: 799.3025 [M+H⁺]. IR: $\tilde{\nu}$ (cm⁻¹) = 2917.0, 2851.9, 1697.9, 1651.7, 1597.9, 1489.0, 1448.8, 1407.3, 1326.5, 1257.1, 1197.6, 1171.5, 1133.1, 1035.9, 984.4, 944.5, 918.5, 893.1. UV-vis (dichloromethane): λ_{ab} (ϵ , M⁻¹cm⁻¹) = 537 nm (5.40 × 10⁴), 503 nm (3.74 × 10⁴), 398 nm (0.96 × 10⁴), [**2**] = 2 × 10⁻⁶ M. Fluorescence (λ_{ex} = 450 nm): λ_{em} = 567 nm (dichloromethane), [**2**] = 2 × 10⁻⁶ M.

N,N'-dicyclohexyl-1,6,7,12-tetraphenoxyperylene-3,4:9,10-tetracarboxylic acid bisimide (**3**): *N,N'*-dicyclohexyl-1,6,7,12-tetrachloroperylene-3,4:9,10-tetracarboxylic acid bisimide (4.14 g, 6 mmol), K₂CO₃ (4.22 g) and phenol (2.82 g, 30 mmol) were added to *N*-methyl pyrrolidone (NMP, 80 mL). The reaction mixture was stirred under argon at 120 °C for 20 h. After cooling to room temperature, the resulting reaction mixture was poured into HCl solution (400 mL, 8 vol %) in water with stirring. The crude product precipitated out and was washed with water then dried under vacuum. The crude product was

purified by silica gel column chromatography with dichloromethane/n-hexane (1/1) as eluent to give red solid (3.98 g). Yield: 72%. ¹H NMR (400 MHz, CDCl₃, ppm, Fig. S10): δ = 8.15 (s, 4H, ArH), 7.26 (t, 8H, ArH), 7.10 (t, 4H, ArH), 6.93 (d, 8H, ArH), 4.92 (t, 2H, 2-CH(CH₂)₂), 2.44 (dd, 4H, 2-CH₂-), 1.83 (d, 4H, 2-CH₂-), 1.67 (d, 6H, 3-CH₂-), 1.37 (dd, 6H, 3-CH₂-). ¹³C NMR (CDCl₃, ppm, Fig. S11): δ = 163.74, 155.90, 155.43, 132.82, 130.0, 127.08, 124.56, 123.21, 120.37, 120.03, 119.98, 54.05, 29.16, 26.55, 25.48. MS (MALDI-TOF, Fig. S12) calculated for C₆₀H₄₆N₂O₈: 922.33; found: 922.11 [M⁺]. IR: $\tilde{\nu}$ (cm⁻¹) = 3040.3, 2929.1, 2852.5, 1691.2, 1649.9, 1585.9, 1486.4, 1412.3, 1341.1, 1285.1, 1199.7, 1166.8, 1075.9, 1024.9, 981.5, 891.1, 871.86. UV-vis absorption (dichloromethane): λ_{ab} (ϵ , M⁻¹cm⁻¹) = 569 nm (4.77 × 10⁴), 530 nm (3.04 × 10⁴), 442 nm (1.65 × 10⁴), [**3**] = 2 × 10⁻⁶ M. Fluorescence (dichloromethane, λ_{ex} = 450 nm): λ_{em} = 603 nm, [**3**] = 2 × 10⁻⁶ M.

3. Results and discussion

3.1. Design and synthesis of π -system perylene dyes

In this work, we synthesized planar perylene dye **1** and two π -twisted dyes **2** and **3** (Fig. 1). Dye **1** is a rigid, planar π -system structure. We initially designed and synthesized a planar perylene bisimide dye with the same cyclohexyl substituent group at imide position as dyes **2** and **3**. However, the solubility of planar perylene dye with the same cyclohexyl group is too poor, which cannot be purified for further measurements. To increase its solubility, we chemically attached long soft polyethylene glycol (PEG) chains to the perylene core at imide position. For dyes **2** and **3**, the perylene π -system planes are twisted by steric hindrance of two and four substitution groups at bay (1,7 and 1,6,7,12) positions, respectively. For dye **2**, we initially designed and synthesized perylene bisimide dye with the same phenoxy substituent group at bay position as dye **3**. However, the perylene dye with the same phenoxy group has a π -twisted angle of only 0–7.1°. This twist angle is too small, which cannot better distinguish with dye **1**. Thus, 3-methoxyphenoxy was used as the substituent group at bay position for dye **2**, where the π -twisted angle is 13.4°. Finally, the average dihedral twist angles between two naphthalene units are ~0°, 13.4° to 27.0° for dyes **1**, **2** and **3**, respectively, according to density functional theory calculations at B3LYP/6-31G (d) level (DFT) (Fig. 1) [40,41].

Dye **1** was synthesized by a five-step reaction procedure (Fig. 2a). The long soft chain PEG-amine was synthesized from the nucleophilic substitution of triethylene glycol monomethylether with *p*-toluene-sulfonyl chloride, and followed by Williamson ether synthesis of 2-(*N,N*-di-benzylamino)-1,3-propanediol and 2-[2-(2-methoxyethoxy) ethoxy] ethyl *p*-toluene sulfonate in the presence of sodium hydride and reduction reaction with the catalysis of Pd/C. Dye **1** was finally obtained through the reaction of PEG-amine with perylene tetracarboxylic acid dianhydride with the catalysis of zinc acetate [42]. The final step reaction has a low synthetic yield of only 16%. The low solubility of starting perylene dianhydrides, and the shielding effect of amine-reactive site by long soft PEG chains may be responsible for low synthetic yield.

Dye **2** was synthesized in a three-step reaction procedure from 1,7-dibromoperylene-3,4:9,10-tetracarboxylic dianhydride, which was obtained through brominated reaction of commercially available 3,4:9,10-perylenetetracarboxylic dianhydride. Imidization of 1,7-dibromoperylene-3,4:9,10-tetracarboxylic dianhydride with cyclohexylamine in the presence of acetic acid in NMP gave corresponding dibromoperylene bisimide. Dye **2** was finally obtained through the nucleophilic substitution reaction of dibromoperylene bisimide with 3-methoxyphenol in the presence of potassium carbonate with a yield of 65% (Fig. 2b). The synthesis of dye **3** started from tetrachloroperylene, i.e. 1,6,7,12-tetrachloro-perylene-3,4:9,10-tetracarboxylic acid dianhydride (Fig. 2c) [32]. By nucleophilic addition-elimination reaction of perylene tetracarboxylic acid dianhydride with cyclohexylamine, the perylene bisimide precursor was obtained with a yield of 92%. The four phenoxy

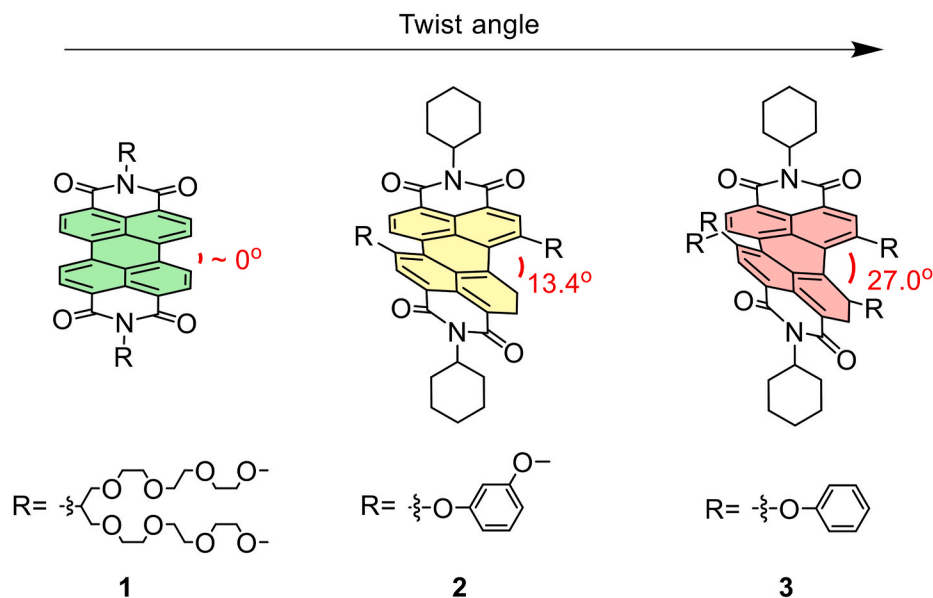


Fig. 1. Chemical structures of perylene bisimide dyes **1**, **2**, **3** with different π -twisted angles.

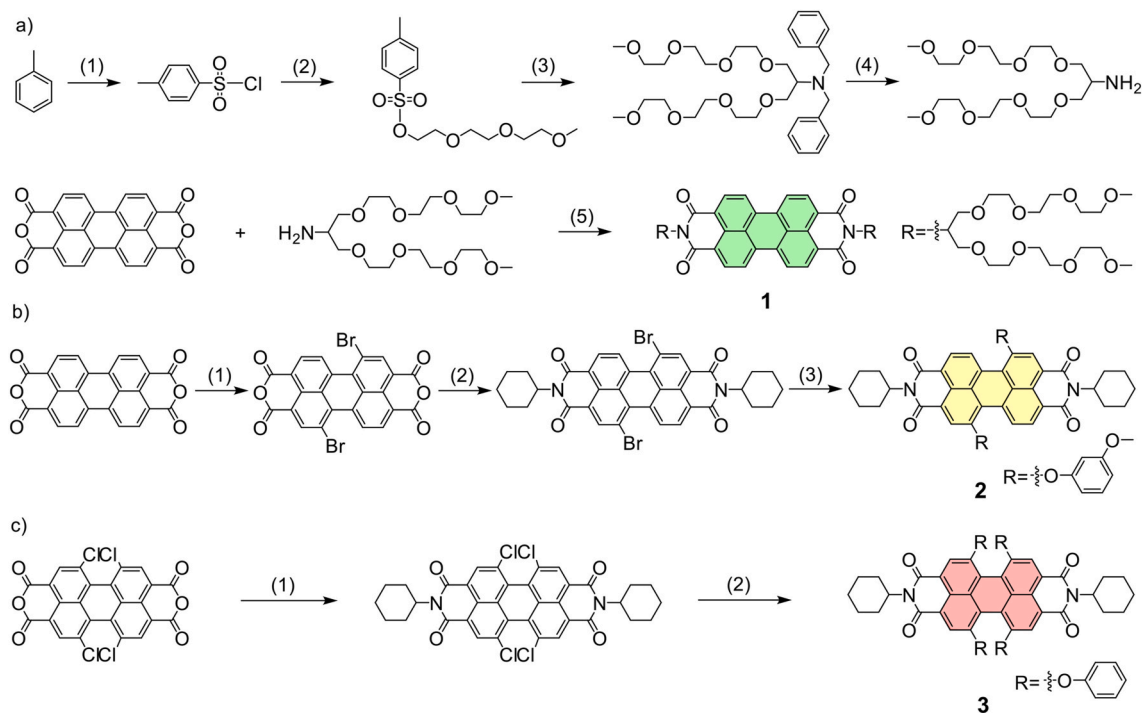


Fig. 2. a) Synthetic route of perylene bisimide dye **1**. Reagents and conditions: (1) HSO_3Cl , 0°C , 4 h, 92%; (2) triethylene glycol monomethylether, Et_3N , CH_2Cl_2 , RT, 20 h, 60%; (3) 2-(*N,N*-di-benzylamino)-1,3-propanediol, NaH , THF, reflux, 16 h, 84%; (4) MeOH , Pd/C , H_2 , 16 h, RT, 72%. (5) Zn (OAc) $_2$, imidazole, 150°C , 6 h, Ar, 16%; b) Synthetic route of dye **2**. Reagents and conditions: (1) H_2SO_4 , I_2 , Br_2 , 85°C , 24 h, 87%. (2) NMP , AcOH , cyclohexylamine, 85°C , 8 h, Ar, 75%. (3) K_2CO_3 , 3-methoxyphenol, NMP , 120°C , 1 h, Ar, 65%; c) Synthetic route of dye **3**. Reagents and conditions: (1) AcOH , cyclohexylamine, NMP , 85°C , 8 h, Ar, 92%. (2) K_2CO_3 , NMP , phenol, 120°C , 20 h, Ar, 72%.

groups were then attached to bay position of perylene core through the nucleophilic substitution reaction of the above tetrachloride perylene bisimide precursor with phenol in the presence of potassium carbonate to give the final dye **3**. Chemical structures of dyes **1**, **2** and **3** were fully characterized by ^1H and ^{13}C NMR spectroscopy, high resolution or MALDI-TOF mass spectroscopy, and IR spectroscopy.

3.2. Optical properties of perylene dye solutions

Highly fluorescent dye solutions have practical applications as optical materials for dye lasers, fluorescence probes and sensors, biological imaging. Thus, we first studied the optical properties of these dye solutions. All these compounds **1**, **2**, **3** display excellent dye absorption characteristics, i.e., high extinction coefficient ($\sim 10^5 \text{ M}^{-1}\text{cm}^{-1}$) within visible-light region. Planar π -system dye **1** shows a well-defined $\text{S}_0\text{-S}_1$ electronic transition absorption band with a maximum wavelength of

525 nm (Fig. 3a). In contrast, the absorption spectra of π -twisted dyes 2 and 3 have no fine structures, and display spectroscopic broadening. An absorption red-shift was observed from 525 nm (dye 1), 537 nm (dye 2) to 569 nm (dye 3) with increasing the π -twisted angles. Thus, we can observe different colours for these dyes under sunlight by naked eyes (Fig. 3a inset). In addition, dye 3 exhibits S_0 - S_2 transition absorption band around 440 nm, which is symmetry-forbidden for planar perylene dyes [43]. We attributed the gradual absorption red-shifts of these dyes to the twisting of conjugated π -system structures, which increases the highest occupied molecular orbital (HOMO) energy level and hence decrease the energy gap between the HOMO and the lowest unoccupied molecular orbital (LUMO) energy levels. The HOMO and LUMO energy gaps (E_g) of these dyes can be obtained from their UV-vis absorption wavelength according to the equation $E_g(\text{eV}) = 1240/\lambda_{\text{ab, onset}}$ [44]. Energy gaps (E_g) decrease in the order of 1 (2.29 eV), 2 (2.18 eV), 3 (2.06 eV) with increasing π -twisted angles. These results were further confirmed by following electrochemical measurements.

These perylene bisimide dyes are highly photoluminescent. Dye 1 has a planar, rigid chromophore structure with high molecular symmetry, which leads to well-resolved, finely structural, three narrow emission bands at 534 nm, 575 nm and 623 nm (Figs. 3b and 4). π -Twisted dyes 2 and 3 show structureless, broad emission bands. Dyes 2 and 3 have π -twisted and flexible structures with lower molecular symmetry, which makes them lose their fine structures of emission bands. Three emission bands cannot be well resolved in dyes 2 and 3

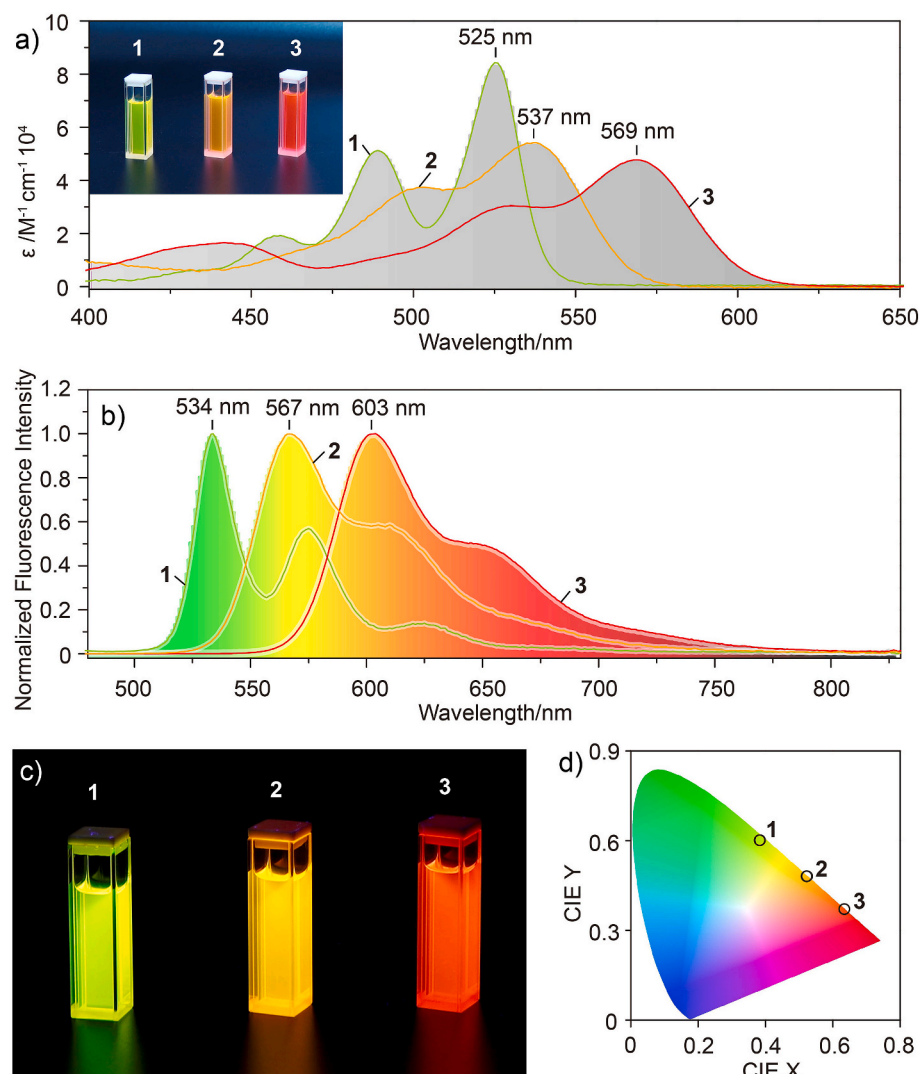


Fig. 3. a) UV-vis absorption spectra of dyes 1, 2, 3 in dichloromethane, Conc: 2×10^{-6} M. Inset: photographs of dichloromethane solutions of dyes 1, 2, 3 under sunlight, Conc: 4×10^{-5} M; b) Fluorescence spectra of dyes 1, 2, 3 in dichloromethane, Conc: 2×10^{-6} M, $\lambda_{\text{ex}} = 450$ nm; c) Photographs of dichloromethane solutions of dyes 1, 2, 3 under 365 nm UV lamp, Conc: 4×10^{-5} M; d) CIE 1931 chromaticity diagram, three points are light-emitting colour coordinates of 1 (0.38, 0.60), 2 (0.52, 0.48) and 3 (0.63, 0.37) in dichloromethane, Conc: 2×10^{-6} M.

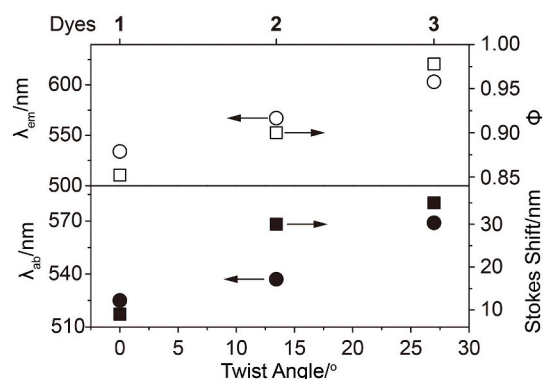


Fig. 4. Changes of optical properties (absorption maximum wavelength (λ_{ab}), emission maximum wavelength (λ_{em}), Stokes shifts and fluorescence quantum yields (Φ)) of dyes 1, 2, 3 with increasing the π -twisted angles.

because that the more flexible conformations cannot be distinguished in their excited states. The emission spectra of these dyes display approximately mirror image relationship with their absorption spectra. The emission bands of these dyes show gradual red-shifts from 534 nm to 603 nm, and Stokes shifts increase from 9 nm to 35 nm with increasing the π -twisted angles. All these emission bands fall within the visible light region. Thus, we can observe different light-emitting colours under UV

lamp, specifically, green, yellow, red (Fig. 3c) for dyes 1, 2, and 3 with light-emitting colour coordinates of (0.38, 0.60), (0.52, 0.48) and (0.63, 0.37), respectively (Fig. 3d). Changes of emission wavelength (colours) of these dyes may be due to the increase in delocalized π -electron area with increasing the π -twisted angles (Table 3).

Interestingly, these dyes are becoming more and more bright with increasing the π -twisted angles, and their fluorescence quantum yields increase from 85.2% to close to 100% (Table 1, Fig. 4). Such highly light-emitting efficiency within visible light region enable us to directly 'see' the emission colours of these dye solutions by naked eyes in the daytime (Fig. 3a inset). Their fluorescence lifetimes slightly increase from 4.2 ns to 6.2 ns from dyes 1 to 3. All optical data of these dye solutions are listed in Table 1. From these optical data, we conclude that the twisting of conjugated π -system structures has a significant influence on their optical properties, especially for light-emitting colour changes. Our light-emitting colour-tunable properties and high emission efficiencies can be considered as a new class of wavelength-tunable dye lasers.

3.3. Environment-sensitive optical probes

We further investigated environment-sensitive ability of these perylene dyes as new fluorescence probes. We measured UV-vis absorption and emission spectra of these dyes in various polarity solvents at very low concentration (2×10^{-6} M) (Fig. 5 and Figs. S13–15). Environment-sensitive ability of these dyes can be quantified by using the following equation [47,48]:

$$\Delta\nu = \nu_A - \nu_F = \frac{2}{hc} \Delta f \frac{(\mu_E - \mu_G)^2}{a^3} + \text{constant} \quad (1)$$

$$\Delta f = \frac{\epsilon - 1}{\epsilon + 2} - \frac{n^2 - 1}{n^2 + 2} \quad (2)$$

where, h is the Planck's constant; c is the speed of light; ν_A and ν_F are the wavenumbers (cm^{-1}) of the absorption and emission, respectively; Δf is the orientation polarizability of solvents; μ_E and μ_G are the dipole moments of dyes in the excited and ground states, respectively; a is the radius of dye fluorophore resides, which is calculated to be 6.13, 6.13 and 6.07 Å for dyes 1, 2, 3, respectively. Stokes shift $\Delta\nu$ ($\Delta\nu = \nu_A - \nu_F$) of all these dyes was plotted against polarity function Δf (Fig. 5). The plot slopes increase from planar dye 1 to π -twisted dyes 2 and 3 (Fig. 5b, d, f). According to the plot slopes and equation (1), we obtained the dipole moment changes ($\Delta\mu = |\mu_E - \mu_G|$), specifically, 2.48 D, 3.89 D and 3.14 D for dyes 1, 2 and 3, respectively. 2.48 D, 3.89 D, 3.14 D are corresponding to the dipole moments of a unit charge separation of 0.52 Å, 0.81 Å, 0.65 Å, respectively. The dipole moment changes ($\Delta\mu$) of these dyes may be due to the decrease in symmetry of π -system structures, and the increase in π -structural flexibility from planar to twisted dyes. A larger dipole moment change ($\Delta\mu$) means the higher environment polarity-sensitive ability. Therefore, the π -twisted perylene dyes are more sensitive to environment changes than planar dye and π -twisted dyes are more excellent fluorescence probes than planar dyes. Compared

Table 1

Average π -twisted angles, UV-vis absorption maximum wavelength (λ_{ab}), extinction coefficient (ϵ), fluorescence emission maximum wavelength (λ_{em}), Stokes shifts, fluorescence quantum yields (Φ) and lifetimes (τ) of dyes 1, 2 and 3 in dichloromethane, Conc: 2×10^{-6} M.

Dyes	Twist angles	λ_{ab}/nm	$\epsilon/\text{M}^{-1}\text{cm}^{-1}$	λ_{em}/nm	Stokes shifts/nm	Φ^a	τ/ns
1	$\sim 0^\circ$	525	8.4×10^4	534	9	0.852	4.2
2	13.4°	537	5.4×10^4	567	30	0.90	4.7
3	27.0°	569	4.8×10^4	603	35	0.978	6.2

^a Fluorescein ($\Phi = 0.95$ in 0.1 N NaOH aqueous solution [45]) and *N, N'*-bis(2,6-diisopropylphenyl)-1,6,7,12-tetraphenoxyperylene-3,4,9,10-tetracarboxylic acid bisimide ($\Phi = 0.96$ in chloroform [46]) were taken as references.

with common fluorescence probes, the advantage of our dyes is high sensitivity to environment changes, which is even directly observable by naked eyes from luminescence colour changes within visible light region.

3.4. Electrochemical properties of *n*-type perylene dyes

We further explore electrochemical properties of our dyes as *n*-type semiconductor or optoelectronic materials due to the electron-deficient π -system structures of perylene bisimide dyes. We performed cyclic voltammetry measurements, these dyes exhibit two reversible reduction waves at negative potentials, which are attributed to the formation of radical anion and dianion of perylene bisimide rings (Fig. 6 and Table 2). Reduction potentials of these dyes decrease in the order of 1 (-0.67 eV) > 2 (-0.85 eV) > 3 (-0.91 eV). These low reduction potentials show that our perylene bisimide dyes are suitable candidate for *n*-type optoelectronic materials.

In addition, planar dye 1 do not show oxidation wave at positive potentials, however, π -twisted dyes 2 and 3 show reversible oxidation waves. Dye 3 displays the lower oxidation potential (1.21 eV). Thus, planar dye 1 is easiest to be reduced and hardest to be oxidized, in contrast, π -twisted dye 3 is relatively hard to be reduced and relatively easy to be oxidized. These conclusions are in good agreement with molecular electrostatic potential calculations, in which the delocalized π electron density of these dyes increases in the order of 1 < 2 < 3. Compared with planar dye 1, the high π electron density of dye 3 is responsible for the large bathochromic shift in its absorption and emission spectra.

The HOMO and LUMO energy levels of these dyes were further calculated by using their redox potentials according to the equations [49]: $E_{\text{LUMO}} = -[4.8 \text{ eV} + E_{1/2} - E_{\text{Fc}/\text{Fc}^+}]$, $E_{\text{HOMO}} = E_{\text{LUMO}} - \Delta E_g$. On the basis of cyclic voltammetry measurement data, HOMO energy levels for dyes 1, 2, 3 were obtained to be -5.95 eV, -5.66 eV, and -5.48 eV, respectively. The LUMO energy levels of dyes 1, 2, 3 were obtained to be -3.66 eV, -3.48 eV and -3.42 eV, respectively, which well falls in the range of organic *n*-type materials for efficient electron injection into the semiconductor [50]. All these experimental data are close to the DFT calculation results (Table 2). HOMO and LUMO energy gaps (ΔE_g) decrease with increasing the π -twisted angles in the order of 1 (2.53 eV) > 2 (2.46 eV) > 3 (2.34 eV) (Fig. 7). The energy gap (ΔE_g) values are fully consistent with those obtained from their UV-vis absorption spectroscopy. The narrowest energy gap for dye 3 well agrees with the energy of its largest absorption wavelength among these dyes.

3.5. Optical properties of dye solids

We further investigated the optical properties of these dye solids, which is desirable for the preparation of optical and optoelectronic devices and materials [51–53]. All these dye solids show emission at 600–850 nm (Fig. 8), which is beyond visible red-light region, and extended to near infra-red (NIR) region. Emission of planar dye 1 extremely changes from its solution to solid state. The solid emission spectrum of dye 1 loses its well-resolved fine structures (Fig. 8a). A new, red-shifted, broad emission band appears at 600–850 nm. Full-width at half maximum (FWHM) of emission spectrum dramatically increases from 21 nm to 156 nm. Emission wavelength shows a large bathochromic shift (131 nm) and fluorescence quantum yield significantly decreases from 85.2% to 9.9% from its solution to solid state (Table 3). All these dramatic optical changes and quenching are attributed to π -stack formation for planar dye 1 from its solution to solid state (Fig. 8b). Dye 1 has a planar π -conjugated structure, which favors a large degree of π - π stacking between adjacent molecules in solid state as observed from X-ray crystal structure of its model compound (Fig. 8b).

In contrast, π -twisted dyes 2 and 3 retain their excellent optical properties in the solid states. Emission spectroscopic shapes and FWHM of dyes 2 and 3 do not obviously change from solution to solid states

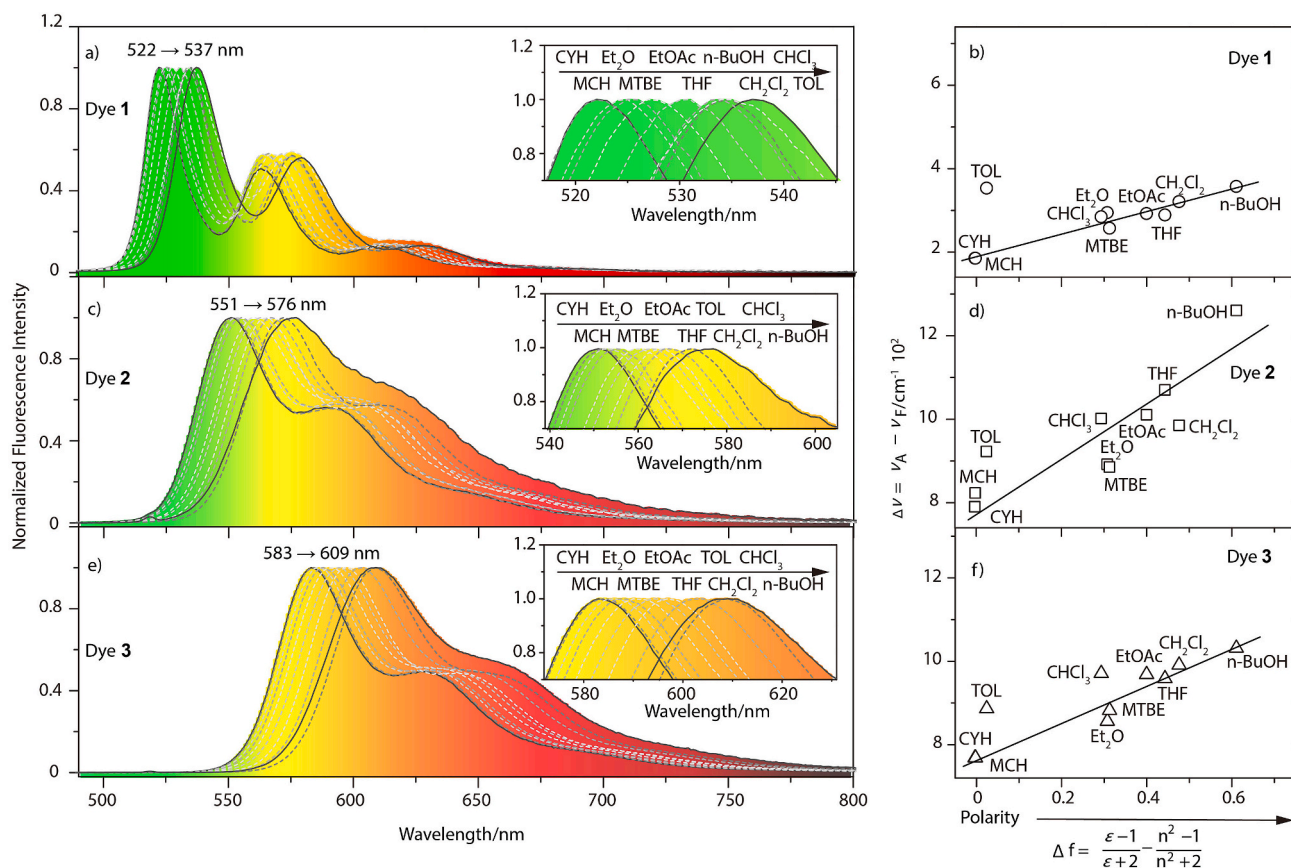


Fig. 5. Environment-sensitive optical properties. Changes of emission spectra and Stokes shifts ($\Delta\nu$) of dyes 1 (a, b), 2 (c, d) and 3 (e, f) with increasing solvent polarity (Δf). Solvents: cyclohexane (CYH), methylocyclohexane (MCH), diethyl ether (Et_2O), methyl *tert*-butyl ether (MTBE), ethyl acetate (EtOAc), tetrahydrofuran (THF), toluene (TOL), dichloromethane (CH_2Cl_2), chloroform (CHCl_3) and *n*-propanol (*n*-BuOH), Conc: 2×10^{-6} M, $\lambda_{\text{ex}} = 450$ nm.

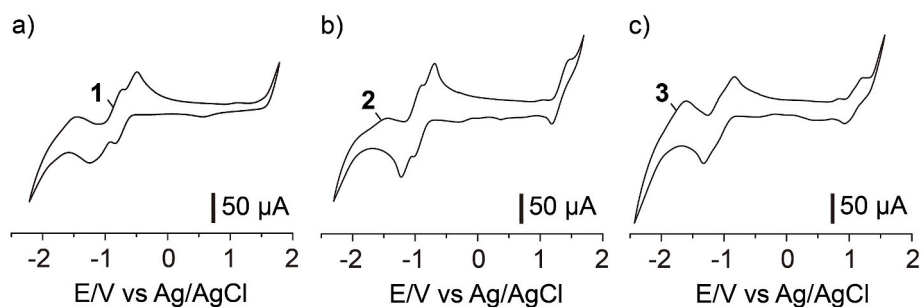


Fig. 6. Cyclic voltammograms of dyes 1, 2, 3, solvent: dichloromethane (0.1 M Bu_4NBF_6), scanning rate: 100 mVs^{-1} (25°C), $c = 0.005$ M.

Table 2

Redox potentials ($E^{+1/2}$, $E_{1/2}$, $E^{2-1/2}$), HOMO and LUMO energy levels, and energy gap (ΔE_g) of dyes 1, 2, 3.

Dyes	$E^{+1/2}$ /V	$E_{1/2}$ /V	$E^{2-1/2}$ /V	HOMO ^b /eV	LUMO ^b /eV	ΔE_g^c /eV	HOMO ^d /eV	LUMO ^d /eV	ΔE_g^d /eV
1	^a	-0.67	-0.99	-5.95	-3.66	2.29	-5.98	-3.45	2.53
2	1.33	-0.85	-1.06	-5.66	-3.48	2.18	-5.61	-3.15	2.46
3	1.12	-0.91	-1.14	-5.48	-3.42	2.06	-5.27	-2.93	2.34

^a No data was obtained.

^b Determined from cyclic voltammetry measurements by using Fc/Fc^+ as a reference. $E_{\text{LUMO}} = -[4.8 \text{ eV} + E_{1/2} - E_{\text{Fc}/\text{Fc}^+}]$, $E_{\text{HOMO}} = E_{\text{LUMO}} - \Delta E_g$, in which $E_{\text{Fc}/\text{Fc}^+}$ is the oxidation potential of ferrocene.

^c $\Delta E_g = 1240/\lambda_{\text{ab, onset}}$.

^d Obtained by the Gaussian calculation based on 6-31G (d).

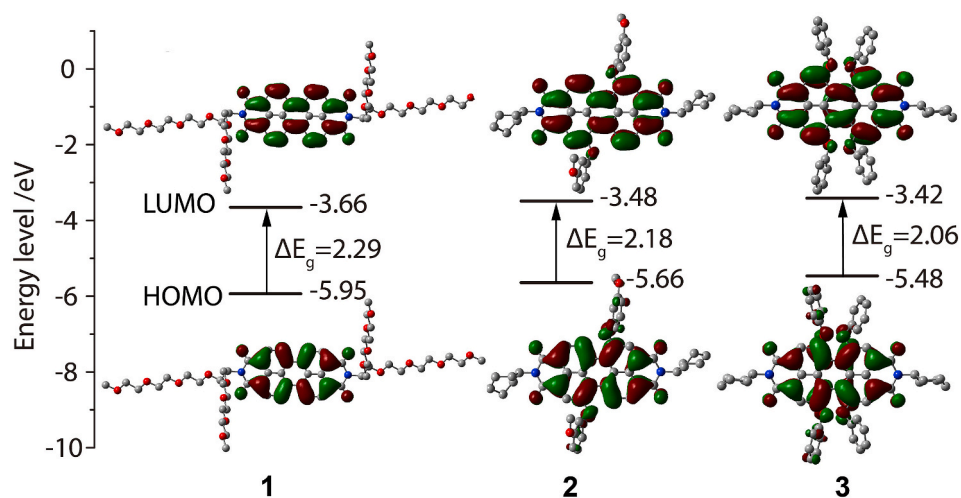


Fig. 7. Energy levels of HOMO and LUMO as well as energy gaps (ΔE_g) of dyes 1, 2, 3 determined from experimental redox potentials of cyclic voltammetry measurements, and electron cloud distribution of dyes 1, 2, 3 obtained by density functional theory calculations at B3LYP/6-31G (d) level.

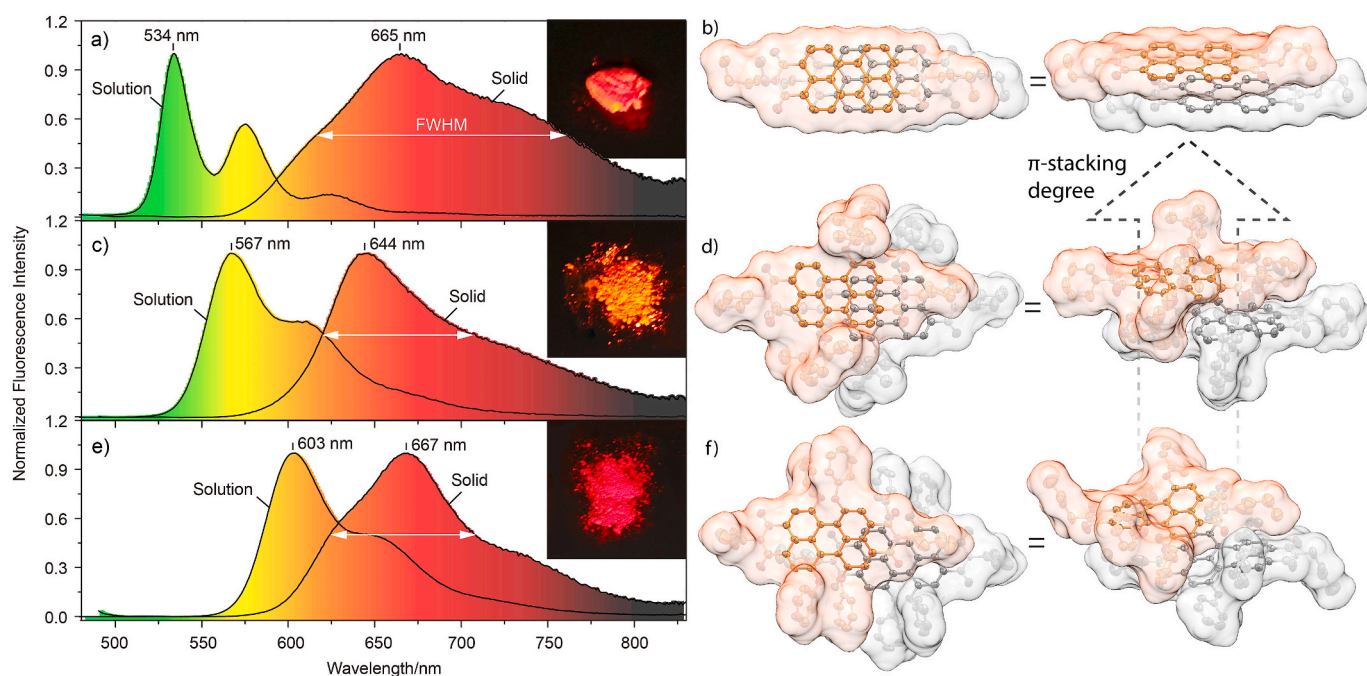


Fig. 8. Emission spectra of dyes 1 (a), 2 (c) and 3 (e) in dichloromethane (Conc: 2×10^{-6} M, $\lambda_{ex} = 450$ nm) and solid states ($\lambda_{ex} = 466$ nm). Inset in (a), (c), (e): photographs of solids of dyes 1, 2, 3 under 365 nm UV lamp. Dye molecular packing structures in solid state determined from single crystal X-ray diffraction of the model compounds [54–56] of dyes 1 (b), 2 (d) and 3 (f).

except for red-shifts in emission wavelength (Fig. 8c and e). The solid emission of largest π -twisted dye 3 displays the smallest emission red-shift (64 nm) from solution to solid states. Solid emission bands of dyes 2 and 3 do not become broad, and remain relatively narrow as their molecularly dissolved monomer state in solution. In the solid state, dyes

2 and 3 remain still highly luminescent, and their fluorescence quantum yields ($\Phi = 32.2\%$ and 21.9%) do not significantly decrease in comparison with their solutions (Table 3). For these π -twisted dyes from their solutions to solid states, relatively, slightly optical changes reveal no distinct structural changes between ground and excited states, and no

Table 3

Average twist angles between two naphthalene units, emission maximum wavelength (λ_{em}), Full-width at half maximum (FWHM) and fluorescence quantum yields (Φ) and anisotropy (r) of dyes 1, 2, 3 in dichloromethane solution and solid states.

Dyes	Twist angle	Delocalized π electron area/ \AA^2	Solution			Solid			
			λ_{em}/nm	FWHM/nm	r	λ_{em}/nm	FWHM/nm	Φ	r
1	$\sim 0^\circ$	36.1	534	21	0	665	156	0.099	~ 0
2	13.4°	36.5	567	71	0	644	104	0.322	0.06
3	27.0°	36.8	603	65	0	667	95	0.219	0.1

π -stacking excimer emission species generate under excited state. Dyes 2 and 3 have twisted, π -conjugated structures, which do not favor π - π stacking in solid state as observed from X-ray crystal structure of their model compounds (Fig. 8d, f). Thus, the solids of dyes 2 and 3 retain similar solution conformations. The emission specie of each molecule is relatively isolated in solid state, and no excited state interaction occurs between adjacent molecules. These prevent efficiently fluorescence quenching. Thus, the solid emissions of π -twisted dyes 2 and 3 still retain outstanding optical properties as their molecularly dissolved monomer states in solution. Our π -twisted dyes are excellent candidates as highly luminescent optical materials. A recent study reported high fluorescence quantum yield dye solids by attaching bulky substituent groups to perylene core at one or two bay positions [34]. Our work is based on a distinctly different viewpoint, that is, a large degree of π -twisting. In particular, our work demonstrates tunable emission colours from green to red, which are not achieved by the method of changing small substituent groups to larger ones at bay positions.

Fluorescence polarization is the phenomenon where light-emitting intensity of a dye is different along different orientation of polarization, which is a very valuable property for optical materials such as liquid crystal displays and optical storage devices [57]. Fluorescence polarization phenomenon of optical dye materials can be quantified by equations (3) and (4) [58]:

$$r = \frac{I_{VV} - GI_{VH}}{I_{VV} + 2GI_{VH}} \quad (3)$$

$$G = \frac{I_{HV}}{I_{HH}} \quad (4)$$

where, I_{VV} and I_{VH} are the fluorescence intensities when the emission polarizer is oriented parallel and perpendicular to the polarization direction of the excitation light, respectively. G factor is the sensitivity ratio of the detection system for vertically and horizontally polarized light.

In general, the anisotropy value of a fluorophore dye is within the ranged between 0.4 (angle between absorption and emission dipole moments is 0°) and -0.2 (angle between absorption and emission dipole moments is 90°) for single photon excitation. We measured fluorescence polarization spectra of our dyes (Fig. 9). No polarization phenomenon was observed for these dye solutions at room temperature. The solid emission of planar dye 1 almost do not also display fluorescence polarization (Fig. 9a). This is because that solid emission of planar dye 1 arose from closely π - π stacking, which leads to coherent energy migration/transfer and a depolarization effect. In contrast, high fluorescence polarization was observed for dyes 2 and 3 (Fig. 9b and c). The anisotropy values increase from 0.06 to 0.1 with increasing π -twisted angles. These interesting fluorescence polarization characteristics of π -twisted dyes can be reasonably interpreted as follows: In the solid states of dyes 2 and 3, their π - π stacking degree is low, dye molecules are loosely packed, and each one is relatively isolated and insulated, and no depolarization effect occurs. All these optical results revealed π -twisted perylene bisimide dyes are more excellent optical materials than planar dyes.

4. Conclusion

In summary, we synthesized three perylene bisimide dyes with different π -twisting degree between two naphthalene units. The twisting of aromatic π -system structures has a remarkable influence on their optical and electrochemical properties, especially for modulation of light-emitting colours of these dyes from green, yellow to red. The optical properties of these dye solutions increase with increasing π -twisted angles. π -Twisted dyes display more excellent fluorescence probe properties than planar dye. In the solid states, planar π -system dye loses its excellent optical characteristics without fluorescence anisotropy due

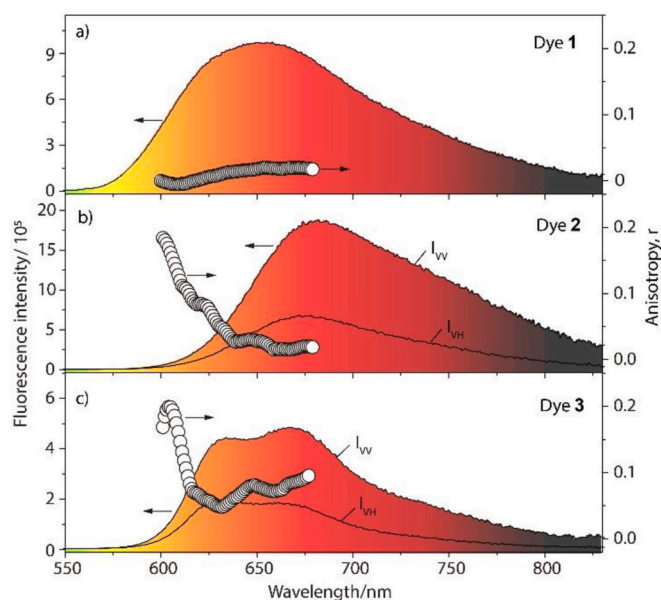


Fig. 9. Fluorescence anisotropy (r , $^\circ$) spectra of dyes 1 (a), 2 (b) and 3 (c) in solid states. I_{VV} and I_{VH} are the fluorescence intensities when the emission polarizer is oriented parallel and perpendicular to the polarization direction of the excitation light, respectively.

to the π - π stacking. In contrast, π -twisted dyes retain their outstanding optical properties with fluorescence polarization phenomenon in the solid states due to the suppression of π - π interactions. Our work provides a rational molecular design guideline from aromatic π -twisting viewpoint to achieve high performance optical materials and optoelectronic devices and materials.

Credit authorship statement

Ying Wang: Data curation, Formal analysis, Investigation, Writing - original draft. **Qi Zhang:** Formal analysis, Investigation, Methodology. **Junbo Gong:** Conceptualization, Funding acquisition, Project administration, Supervision. **Xin Zhang:** Conceptualization, Supervision, Writing - review & editing.

Declaration of competing interest

The authors declare that they have no known competing financial interests or personal relationships that could have appeared to influence the work reported in this paper.

Acknowledgements

National Natural Science Foundation of China (grant number 21975177 and 21674079) is acknowledged for financial support.

Appendix A. Supplementary data

Supplementary data to this article can be found online at <https://doi.org/10.1016/j.dyepig.2021.109261>.

References

- [1] Xu Z, Singh NJ, Lim J, Pan J, Kim HN, Park S, Kim KS, Yoon J. Unique sandwich stacking of pyrene-adenine-pyrene for selective and ratiometric fluorescent sensing of ATP at physiological pH. *J Am Chem Soc* 2009;131:15528–33.
- [2] Pramanik P, Ray D, Aswal VK, Ghosh S. Supramolecularly engineered amphiphilic macromolecules: molecular interaction overrules packing parameters. *Angew Chem Int Ed* 2017;56:3516–20.

- [3] Dou SL, Wang Y, Zhang X. Amphiphilic fluorescence resonance energy-transfer dyes: synthesis, fluorescence, and aggregation behavior in water. *Chem Eur J* 2020; 26:11503–10.
- [4] Sato O. Dynamic molecular crystals with switchable physical properties. *Nat Chem* 2016;8:644–56.
- [5] Ma CP, Zhang XQ, Yang Y, Ma ZY, Yang LT, Wu YJ, Liu HL, Jia XR, Wei Y. Effect of alkyl length dependent crystallinity for the mechanochromic feature of alkyl phenothiazinyl tetraphenylethynyl acrylonitrile derivatives. *J Mater Chem C* 2016; 4:4786–91.
- [6] Zhu MQ. Both self-assembly and aggregation-induced emission are photoswitchable. *Sci China Chem* 2018;61:1201–2.
- [7] Ghosh G, Dey P, Ghosh S. Controlled supramolecular polymerization of pi-systems. *Chem Commun* 2020;56:6757–69.
- [8] Uesaka T, Ishitani T, Sawada R, Maeda T, Yagi S. Fluorescent 2-phenyl-2H-benzotriazole dyes with intramolecular N-H center dot center dot N hydrogen bonding: synthesis and modulation of fluorescence properties by proton-donating substituents. *Dyes Pigments* 2020;183. 108672.
- [9] Yang Y, Zhang S, Zhang X, Gao L, Wei Y, Ji Y. Detecting topology freezing transition temperature of vitrimers by AIE luminogens. *Nat Commun* 2019;10: 3165.
- [10] Wang Y, Zhang Q, Li F, Gong JB, Zhang X. Donor/acceptor maleimide and itaconimide dyes: synthesis, fluorescence and electrochemical properties. *Dyes Pigments* 2020;172. 107823.
- [11] Yang SK, Shi X, Park S, Doganay S, Ha T, Zimmerman SC. Monovalent, clickable, uncharged, water-soluble perylene-diimide-cored dendrimers for target-specific fluorescent biolabeling. *J Am Chem Soc* 2011;133:9964–7.
- [12] Blechinger J, Herrmann R, Kiener D, Garcia-Garcia FJ, Scheu C, Reller A, Brauchle C. Perylene-labeled silica nanoparticles: synthesis and characterization of three novel silica nanoparticle species for live-cell imaging. *Small* 2010;6:2427–35.
- [13] Ramírez MG, Pla S, Boj PG, Villalvilla JM, Quintana JA, Sastre-Santos A. 1,7-bay-substituted perylene-diimide derivative with outstanding laser performance. *Adv Opt Mater* 2013;1:933–8.
- [14] Matussek M, Filapek M, Gancarz P, Krompiec S, Malecki JG, Kotowicz S, Siwy M, Mackowski S, Chrobok A, Schab-Balcerzak E, Slodek A. Synthesis and photophysical properties of new perylene bisimide derivatives for application as emitting materials in OLEDs. *Dyes Pigments* 2018;159:590–9.
- [15] Kozma E, Catellani M. Perylene diimides based materials for organic solar cells. *Dyes Pigments* 2013;98:160–79.
- [16] Zhou EJ, Cong JZ, Wei QS, Tajima K, Yang CH, Hashimoto K. All-Polymer solar cells from perylene diimide based copolymers: material design and phase separation control. *Angew Chem Int Ed* 2011;50:2799–803.
- [17] Ding ZC, Zhao RY, Yu YJ, Liu J. All-polymer indoor photovoltaics with high open-circuit voltage. *J Mater Chem A* 2019;7:26533–9.
- [18] Prasanthkumar S, Ghosh S, Nair VC, Saeki A, Seki S, Ajayaghosh A. Organic donor-acceptor assemblies form coaxial p-n heterojunctions with high photoconductivity. *Angew Chem Int Ed* 2015;54:946–50.
- [19] Maeda T, Nguyen TV, Kuwano Y, Chen XX, Miyana K, Nakazumi H, Yagi S, Soman S, Ajayaghosh A. Intramolecular exciton-coupled squaraine dyes for dye-sensitized solar cells. *J Phys Chem C* 2018;122:21745–54.
- [20] Tarafdar G, Pandey UK, Sengupta S, Ramamurthy PC. Effect of structural isomerism in BODIPY based donor-acceptor co-polymers on their photovoltaic performance. *Sol Energy* 2019;186:215–24.
- [21] Han H, Ma LK, Zhang L, Guo YK, Li YK, Yu H, Ma W, Yan H, Zhao DH. Tweaking the molecular geometry of a tetraperylene-diimide acceptor. *ACS Appl Mater Interfaces* 2019;11:6970–7.
- [22] Liu C, Xiao C, Li Y, Hu W, Li Z, Wang Z. High performance, air stable n-type single crystal transistors based on core-tetrachlorinated perylene diimides. *Chem Commun* 2014;50:12462–4.
- [23] Schmidt R, Oh JH, Sun YS, Deppisch M, Krause AM, Radacki K, Braunschweig H, Konemann M, Erk P, Bao ZA, Würthner F. High-performance air-stable n-channel organic thin film transistors based on halogenated perylene bisimide semiconductors. *J Am Chem Soc* 2009;131:6215–28.
- [24] Li XH, Wang Y, Li F, Zhang X. Fluorescent carbazole-containing dyes: synthesis and supramolecular assembly by self-complementary donor-acceptor pi-stacking and dipolar interactions. *Dyes Pigments* 2020;182. 108474.
- [25] Zhang X, Rehm S, Safont-Sempere MM, Würthner F. Vesicular perylene dye nanocapsules as supramolecular fluorescent pH sensor systems. *Nat Chem* 2009;1: 623–9.
- [26] Chen T, Chen Z-Q, Gong W-L, Li C, Zhu M-Q. Ultrasensitive water sensors based on fluorenone-tetraphenylethene AIE luminogens. *Mater Chem Front* 2017;1:1841–6.
- [27] Aswathy PR, Sharma S, Tripathi NP, Sengupta S. Regioisomeric BODIPY benzodithiophene dyads and triads with tunable red emission as ratiometric temperature and Viscosity sensors. *Chem Eur J* 2019;25:14870–80.
- [28] Sun NN, Wang CM, Wang HL, Yang L, Jin P, Zhang W, Jiang JZ. Multifunctional tubular organic cage-supported ultrafine palladium nanoparticles for sequential catalysis. *Angew Chem Int Ed* 2019;58:18011–6.
- [29] Rajdev P, Ghosh S. Fluorescence resonance energy transfer (FRET): a powerful tool for probing amphiphilic polymer aggregates and supramolecular polymers. *J Phys Chem B* 2019;123:327–42.
- [30] Handa NV, Mendoza KD, Shirtcliff LD. Syntheses and properties of 1,6 and 1,7 perylene diimides and tetracarboxylic dianhydrides. *Org Lett* 2011;13:4724–7.
- [31] Zhen Y, Wang C, Wang Z. Tetrachloro-tetra(peryene bisimides): an approach towards N-type graphene nanoribbons. *Chem Commun* 2010;46:1926–8.
- [32] Schill J, van Dun S, Pouderoijen MJ, Janssen HM, Milroy L-G, Schenning APHJ, Brunsveld L. Synthesis and self-assembly of bay-substituted perylene diimide gemini-type surfactants as off-on fluorescent probes for lipid bilayers. *Chem Eur J* 2018;24:7734–41.
- [33] Schill J, Schenning APHJ, Brunsveld L. Self-assembled fluorescent nanoparticles from -conjugated small molecules: en route to biological applications. *Macromol Rapid Commun* 2015;36:1306–21.
- [34] Stolte M, Schembri T, Sues J, Schmidt D, Krause A-M, Vysotsky MO, Wuerthner F. 1-mono- and 1,7-disubstituted perylene bisimide dyes with voluminous groups at bay positions: in search for highly effective solid-state fluorescence materials. *Chem Mater* 2020;32:6222–36.
- [35] Chen Z, Baumeister U, Tschierske C, Wuerthner F. Effect of core twisting on self-assembly and optical properties of perylene bisimide dyes in solution and columnar liquid crystalline phases. *Chem Eur J* 2007;13:450–65.
- [36] Lou AJT, Marks TJ. A twist on nonlinear optics: understanding the unique response of pi-twisted chromophores. *Accounts Chem Res* 2019;52:1428–38.
- [37] Zhang X, Goerl D, Stepanenko V, Wuerthner F. Hierarchical growth of fluorescent dye aggregates in water by fusion of segmented nanostructures. *Angew Chem Int Ed* 2014;53:1270–4.
- [38] Gorl D, Zhang X, Stepanenko V, Würthner F. Supramolecular block copolymers by kinetically controlled co-self-assembly of planar and core-twisted perylene bisimides. *Nat Commun* 2015;6:7009–16.
- [39] Li F, Li X, Wang Y, Zhang X. Trismaleimide dendrimers: helix-to-superhelix supramolecular transition accompanied by white-light emission. *Angew Chem Int Ed* 2019;58:17994–8002.
- [40] Peng MD, Wang Y, Zhang X. Pyrene-containing dyes: reversible click/declick reaction, optical and aggregation behaviors. *Dyes Pigments* 2020;179. 108375.
- [41] Huang L, Liu L, Li X, Hu H, Chen M, Yang Q, Ma Z, Jia X. Crystal-state photochromism and dual-mode mechanochromism of an organic molecule with fluorescence, room-temperature phosphorescence, and delayed fluorescence. *Angew Chem Int Ed* 2019;58:16445–50.
- [42] Schill J, Milroy L-G, Lugger JAM, Schenning APHJ, Brunsveld L. Relationship between side-chain polarity and the self-assembly characteristics of perylene diimide derivatives in aqueous solution. *Chemistry Open* 2017;6:266–72.
- [43] Sadrai M, Hadel L, Sauer RR, Husain S, Krogh-Jespersen K, Westbrook JD, Bird GR. Lasing action in a family of perylene derivatives: singlet absorption and emission spectra, triplet absorption and oxygen quenching constants, and molecular mechanics and semiempirical molecular orbital calculations. *J Phys Chem* 1992;96:7988–96.
- [44] Al-Khateeb B, Dinleyici M, Abourajab A, Kok C, Bodapati JB, Uzun D, Koyuncu S, Icil H. Swallow tail bay-substituted novel perylene bisimides: synthesis, characterization, photophysical and electrochemical properties and DFT studies. *J Photochem Photobiol Chem* 2020:393.
- [45] Brannon JH, Magde D. Absolute quantum yield determination by thermal blooming. *Fluorescein J Phys Chem* 1923;82:705–9.
- [46] Gvishi R, Reisfeld R, Burshtein Z. Spectroscopy and laser action of the “red perylimide dye” in various solvents. *Chem Phys Lett* 1993;213:338–44.
- [47] McRae EG. Theory of solvent effects on molecular electronic spectra. Frequency shifts. *J Phys Chem* 1957;61:562–72.
- [48] Yadav SB, Kothavale S, Sekar N. Triphenylamine and N-phenyl carbazole-based coumarin derivatives: synthesis, solvatochromism, acidochromism, linear and nonlinear optical properties. *J Photochem Photobiol Chem* 2019;382:19.
- [49] Miao J, Wang J, Meng B, Liu J, Wang L. An A-D-A'-D-A type small molecule acceptor with wide absorption spectrum and near-infrared absorption. *Mater Chem Front* 2018;2:2333–9.
- [50] Jones BA, Faccetti A, Wasielewski MR, Marks TJ. Tuning orbital energetics in arylene diimide semiconductors. Materials design for ambient stability of n-type charge transport. *J Am Chem Soc* 2007;129:15259–78.
- [51] Ma Z, Li A, Huang L, Qiu Y, Xu S, Xu W, Jia X. Photochromism of aminobenzopyrano-xanthene with different fluorescent behavior in solution and the crystal state. *J Mater Chem C* 2019;7:275–80.
- [52] Morisue M, Hoshino Y, Shimizu M, Nakanishi T, Hasegawa Y, Hossain MA, Sakurai S, Sasaki S, Uemura S, Matsui J. Supramolecular polymer of near-infrared luminescent porphyrin glass. *Macromolecules* 2017;50:3186–92.
- [53] Suzuki M, Sakata T, Takenobu R, Uemura S, Miyagawa H, Nakanishi S, Tsurumachi N. Dye concentration dependence of spectral triplet in one-dimensional photonic crystal with cyanine dye J-aggregate in strong coupling regime. *Appl Phys Lett* 2017;111. 163302.
- [54] Mizuguchi J. Crystal structure of a second modification of N,N'-di-n-butylperylene-3,4 : 9,10-bis(dicarboximide), C₃₂H₂₆N₂O₄. *Z Krist-New Cryst St* 2003;218:131–3.
- [55] Jimenez AJ, Lin M-J, Burschka C, Becker J, Settels V, Engels B, Wuerthner F. Structure-property relationships for 1,7-diphenoxy-peryene bisimides in solution and in the solid state. *Chem Sci* 2014;5:608–19.
- [56] Pinto RM, Macoas EMS, Neves AIS, Raja S, Baleizao C, Santos IC, Alves H. Effect of molecular stacking on exciton diffusion in crystalline organic semiconductors. *J Am Chem Soc* 2015;137:7104–10.
- [57] Joseph RL. Principles of fluorescence spectroscopy. third ed. New York: Springer Academic Business Media; 2006.
- [58] Menelaou C, ter Schiphorst J, Kendhale AM, Parkinson P, Debije MG, Schenning AP, Herz LM. Rapid energy transfer enabling control of emission polarization in perylene bisimide donor-acceptor triads. *J Phys Chem Lett* 2015;6: 1170–6.